Multiphysics NVH Modeling: Simulation of a Switched Reluctance Motor for an Electric Vehicle

Fábio L. M. dos Santos, Jan Anthonis, Francesco Naclerio, Johan J. C. Gyselinck, *Member, IEEE*, Herman Van der Auweraer, *Member, IEEE*, and Luiz C. S. Góes

***Abstract*—This paper presents a multiphysics modeling of a switched reluctance motor (SRM) to simulate the acoustic radiation of the electrical machine. The proposed method uses a 2-D finite-element model of the motor to simulate its magnetic properties and a multiphysics mechatronic model of the motor and controls to simulate operating conditions. Magnetic forces on the stator are calculated using finite-element analysis and are used as the excitation on a forced response analysis that contains a finite-element model of the motor stator structure. Finally, sound power levels are calculated using the boundary element method. Simulation results of the model are shown and compared with experimental measurements for a four-phase 8/6 SRM.**

***Index Terms*—Acoustic noise, finite-element analysis (FEA), multiphysics modeling, switched reluctance motor (SRM).**

I. Introduction

THE DESIGN and simulation of switched reluctance motors (SRMs) has increasingly become the attention of both industry and academia. This sort of motor is an attractive option for electric vehicle (EV) systems [1], [2] due to their inherent robustness and high efficiency [3] as well as their independence from permanent magnets and windings on the rotor, making them more suitable for severe environments. On the other hand, this type of motor is known for having high vibration and acoustic noise levels [4], [5], which can make for prohibitive use in EVs, so predicting its acoustic properties at an early design stage can be substantially beneficial [6].

There is a relevant amount of studies on the modeling, vibration, and acoustic radiation of the SRM. A review on the SRM modeling is shown in [7], where various methods of analyzing the machine are compared. The vibration transmission and noise radiation of the stator are calculated analytically in [8], by means of modal superposition, and a computational analysis comparing different frame geometry and materials is carried out in [9], followed by prototyping and acoustic measurements.

It is well known that most of the noise generated from the SRM comes from structural vibration due to electromagnetic air-gap forces acting on the stator [10]. In [11], these forces are calculated via electromagnetic finite-element analysis (FEA). Furthermore, a numerical modal analysis of the stator is performed via structural FEA in [12] to obtain the surface vibrations on the motor. Acoustic radiation is simulated in [13], where a field-circuit approach is used and the sound power level is simulated using a boundary element method (BEM). Similar multiphysics system studies have been carried out for a permanent-magnet synchronous machine [14] and for a pulse-width modulation (PWM)-fed induction machine [15].

In this study, a multiphysics model of an SRM is developed, with the main focus on the vibroacoustic behavior prediction and experimental validation. For this purpose, an electromagnetic model of the SRM is created using a 2-D electromagnetic FEA, to obtain important flux and torque characteristics of the system [16], as opposed to an analytical approach [17], [18]. This model is used in a 1-D mechatronic simulation system that can include reference tracking, angle control, and loads. Then, the vibroacoustic behavior of the SRM is simulated by means of structural FEA, and sound radiation is calculated via BEM, with experimental validation being carried out in different steps of the method.

An overall diagram for the acoustic prediction methodology is represented in Fig. 1. Each level of the diagram represents a simulation run in the methodology, and the arrows between levels indicate parameters used on the next part. Considering a four-phase motor, $\theta[t]$ is the SRM rotor position for a given simulation, $I_{1,2,3,4}[t]$ are the phase currents, and F_y and F_x are the forces exerted on the stator poles.

This paper is structured as follows. First, a brief introduction on the SRM characteristics and modeling method is given, and the 1-D mechatronic system is explained as well. Then, the vibroacoustic model of the motor stator is detailed. Finally, simulation and experimental results are compared for the 1-D system, using time and frequency data. Subsequently, a comparison between the vibroacoustic experimental and simulated systems is realized, by examining both sets' sound power level spectra.

II. SRM Characteristics and Model

Some particular features are present in the SRM—neither stator nor rotor contains permanent magnets. Instead, the stator

Manuscript received April 5, 2012; revised September 21, 2012 and January 3, 2013; accepted January 17, 2013. Date of publication February 13, 2013; date of current version July 18, 2013. This work was supported in part by the IWT Agency for Innovation by Science and Technology and in part by the Flanders' Drive Organization.

F. L. M. dos Santos, J. Anthonis, F. Naclerio, and H. Van der Auweraer are with LMS International, 3001 Leuven, Belgium (e-mail: fabio.santos@lmsintl.com; jan.anthonis@lmsintl.com; francesco.naclerio@lmsintl.com; herman.vanderauweraer@lmsintl.com).

J. J. C. Gyselinck is with the Université Libre de Bruxelles-BEAMS, B1050 Brussels, Belgium (e-mail: Johan.Gyselinck@ulb.ac.be).

L. C. S. Góes is with the Instituto Tecnológico de Aeronáutica, 12228-900 São José dos Campos, Brazil (e-mail: goes@ita.br).

Color versions of one or more of the figures in this paper are available online at http://ieeexplore.ieee.org.

Digital Object Identifier 10.1109/TIE.2013.2247012

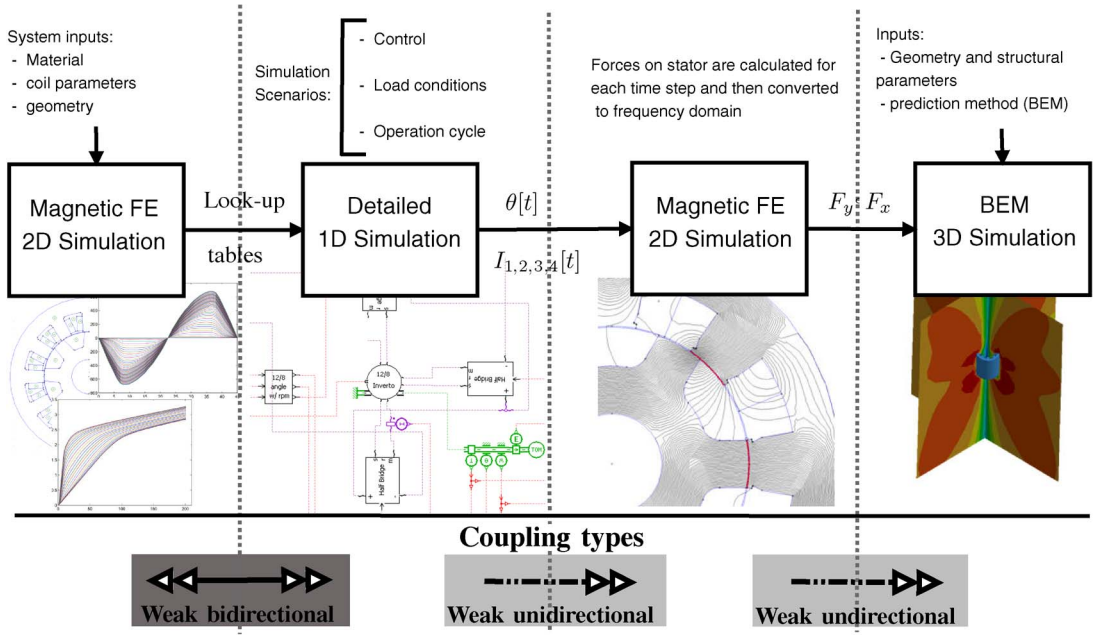

Fig. 1. Acoustic prediction diagram.

poles contain windings that generate a magnetic field when energized. Motion is generated by the tendency of the rotor to turn to the position of minimum reluctance in the air gap between stator and rotor poles. By energizing opposite poles in the stator consecutively, continuous rotation is achieved.

A. SRM Design for an EV

The motor investigated in this study has eight stator poles (four stator pole pairs) and six rotor poles, and thus is an 8/6 SRM, with four independent phases. Its cross section is shown in Fig. 3(a). The motor was designed for automotive traction applications and has the following specifications [19]:

1) peak torque: 200 N · m;
2) peak power: 30 kW;
3) speed range: 0–10 000 r/min;
4) continuous power: 15 kW.

This motor is a prototype in design phase. A first test of the motor was carried out in a front-wheel-driven EV [20]. Some road tests were done in order to assess the vibroacoustic behavior of the motor in an EV. Fig. 2 shows acoustic measurements carried out in the wide open throttle (WOT) condition, where the vehicle was accelerated from 0 to 160 km/h. The diagonal dark lines represent the motor orders, i.e., speed-dependent behavior, and the vertical dark area around 1400 Hz is a behavior most likely related to a structural resonance. It is also important to notice how the order lines are amplified when they pass through this 1400-Hz area. The overall acoustic behavior of the motor was not satisfactory, which led to this study to better understand its characteristics.

B. Electromagnetic Equations

The applied voltage on a phase of the SRM is related to the flux linkage and to the current passing through the coil,

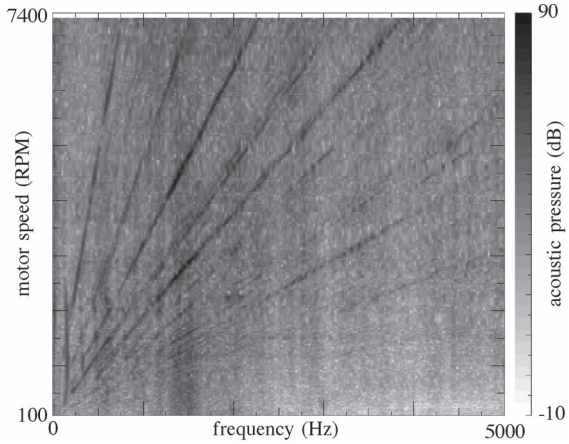

Fig. 2. EV WOT test—acoustic measurements on driver's seat.

according to Faraday's law

$$v_k = \frac{d\lambda_k}{dt} + R_s i_k \tag{1}$$

where v is the terminal voltage, i is the current, λ is the flux linkage, R_s is the phase resistance, and the index $k = \{1, 2, 3, 4\}$ represents the phase number. Mutual coupling between phases is considered very small and is therefore neglected. The flux linkage of the SRM phase changes as the rotor turns [21] and as the current changes [22]. Therefore, the term $d\lambda_k/dt$ in (1) can be expanded

$$v_k = \frac{\partial \lambda_k}{\partial i_k}\frac{di_k}{dt} + \frac{\partial \lambda_k}{\partial \theta}\frac{d\theta}{dt} \tag{2}$$

with $\partial\lambda_k/\partial i_k$ being defined as the incremental inductance $L(\theta, i_k)$, and the induced electromotive force is defined as $(\partial\lambda_k/\partial\theta)(d\theta/dt)$. The phase torque can be obtained by calculating the magnetic forces acting on the rotor. These forces can be distinguished in two categories—forces acting on the

surface of the medium and forces that act on the volume of the medium. The latter is usually negligible with respect to the surface density forces [13]. Then, the Maxwell stress tensor can be used to define the force density (or force distribution) with its normal and tangential components [12]

$$F_e = \frac{1}{2\mu_0}\left(B_n^2 - B_t^2\right)\vec{n} + \frac{1}{\mu_0}B_n B_t \vec{t} \tag{3}$$

where μ_0 is the magnetic permeability of vacuum and B_n and B_t are the flux densities in the normal and tangential directions, with $\vec{n}$ and $\vec{t}$ representing the radial and tangential components on the considered surface. This force, in turn, is calculated by integrating the stress tensor over the desired surface. The integration of (3) over the surface is done via FEA, which is also used to obtain flux and current values. The torque contribution due to each phase is obtained from the tangential forces acting on the rotor, and the lookup tables can be populated. The total motor torque is the sum of all phase torques

$$\tau_e(i_1, i_2, i_3, i_4, \theta) = \sum_{k=1}^{4} \tau_k(i_k, \theta). \tag{4}$$

At each simulation step $[n]$, $\theta[n]$ and $\lambda_{k=1:4}[n]$ are used to look up the values of $i_{k=1:4}[n+1]$, which are then used to obtain $\tau_{k=1:4}[n+1]$. Finally, the next step $\lambda_{k=1:4}[n+1]$ is obtained through the integration of (1), with $v_{k=1:4}[n+1]$ as input, and $\theta[n+1]$ is obtained through the double integration of the mechanical relation between τ_e and the angular acceleration

$$\theta = \frac{1}{J}\int\left[\int\left(\tau_e - \tau_{load}\right)dt\right]dt \tag{5}$$

where J is the rotor total moment of inertia and τ_{load} is the load torque.

The full lookup table data of the motor are obtained by running several electromagnetic FEA simulations, where torque and flux linkage information is obtained for a discretized number of rotor angles and phase current values [23]. Magnetic hysteresis is not taken into account in this. This effect should introduce damping in the magnetic circuit [24] and was not considered in this study.

This SRM model is, in turn, used in a 1-D mechatronic simulation environment, where the SRM system can be complemented by power electronics, angle activation, controls, loads, etc. The complete system is able to provide detailed data on phase currents in function of the rotor position, which, in turn, can be used to evaluate firing angle strategies [25] or control techniques [26]. Inputs to the model are the voltages applied in each individual phase and the rotational velocity of the load. Fig. 3 shows the system with causality.

The full 1-D system schematic is shown in Fig. 4. It includes the SRM plus load, asymmetric half-bridge power electronics, angle conversion for the activation of individual phases, and hysteresis current control [27]. It should be noted that the SRM model has an additional input that can be used for temperature-dependent simulations, which is not considered in this work.

Coupling between the magnetic and the electrical system in this case is considered to be weak and bidirectional [14]. That

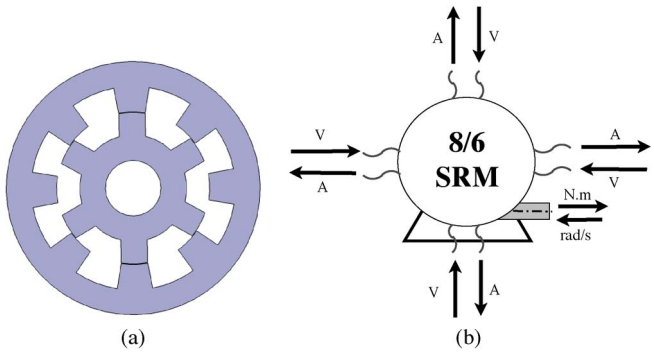

Fig. 3. SRM (a) cross section and (b) causality model—the four SRM phases have voltage as input and current as output, and the shaft has angular velocity as input and torque as output. (a) 8/6 SRM cross section. (b) SRM mechatronic model with causality.

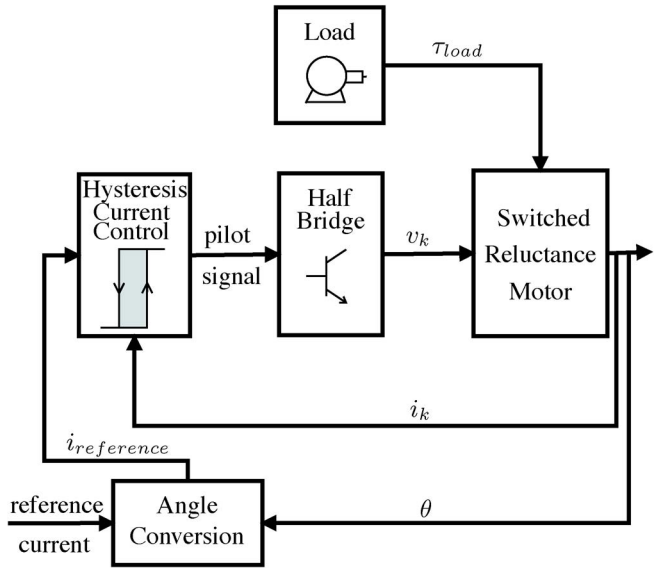

Fig. 4. Block diagram representing SRM control scheme and load.

is, there is exchange of information between the magnetic and the electrical systems, but the magnetic FEA is not rerun, and only the lookup tables are used. Fig. 1 also shows the coupling type and directions for the other considered systems.

III. Vibroacoustic Analysis

Vibration and noise from the SRM comes mainly from the stator deformation, induced by the constantly varying magnetic field activating individual phases. The deformation on the outer surface of the motor causes the air around it to move, generating pressure differences, which are perceived as noise for the human ear. There are three domains to be considered in this analysis—magnetic, vibrational (structural), and acoustic.

The couplings considered in this simulation part are between the magnetic and vibrational systems and between the vibrational and acoustic systems. Both of these couplings are approximated to be weak and unidirectional. That is, the magnetic field generates a change in the structural system, but this change is not significant to affect the magnetic field itself (by deforming the magnetic core). The same is true for the structural and acoustic coupling—the air that is moved around the stator does

not affect the vibration of the stator itself. Refer to Fig. 1 for the respective system couplings.

Forces acting on the surface of the stator poles are calculated by means of the Maxwell stress tensor, as described in (3), and they are the excitation in the structural model. The equation of motion of a multiple-degree-of-freedom structural system can be represented as

$$[M]\{\ddot{x}(t)\} + [C]\{\dot{x}(t)\} + [K]\{x(t)\} = \{F(t)\} \quad (6)$$

where M, C, and K are the global mass, damping, and stiffness matrices, $x(t)$ is the displacement at a given degree of freedom in the structure, and $F(t)$ is the excitation force. The structural damping of the motor stator is usually quite low and therefore is usually neglected [13]. The solution of (6) with $C = 0$ can obtained via the eigenvalue problem

$$\left([K] - \omega^2[M]\right)\{X(\omega)\} = 0. \quad (7)$$

The resulting eigenmodes are orthogonal functions, so the system response can be represented by a linear combination of these modes, which leads to the essential modal analysis equation [28]

$$X(\omega) = \sum_{r=1}^{n} \frac{\Phi_r^T F(\omega)\Phi_r}{\omega_r^2 - \omega^2}. \quad (8)$$

The vibration modes of the stator can be obtained by different methods, such as analytical approximations [8], by using experimental modal analysis [10] or using 3-D FEA of the stator [9]. The latter method is used in this work. A model of the motor stator that uses an approximate stator pole geometry, does not take into account the lamination of the stack, and neglects the coil mass was used for this purpose.

To predict the acoustic radiation efficiency of the motor, the indirect BEM [29], [30] was used. This method finds the solution to the second-order Helmholtz equation

$$\nabla^2 p(x,y,z) + k^2 p(x,y,z) = -j\rho_0\omega q(x,y,z) \quad (9)$$

where p is the acoustic pressure at a point (x, y, z) due to a time-harmonic source distribution q at frequency ω, with the wavenumber $k = \omega/c$, c being the speed of sound, and ρ_0 being the fluid density [31]. The method considers a discretized closed boundary surface and uses the surface's normal velocities as boundary conditions. Additionally, for exterior acoustic problems, an additional boundary condition is used, viz., the Sommerfeld radiation condition. This boundary surface is located at infinity, and it ensures that all waves propagate freely without any reflections at the boundary. Equation (9) is solved numerically only for the boundary of the acoustic domain and for a discrete number of frequencies.

This method is computationally more advantageous when compared with the finite-element method for exterior acoustics problems, because there is no need to model the air volume around the stator, so only a surface around the SRM stator is discretized. The stator surface accelerations are estimated by the forced response of the 3-D stator structural model, the radiating body is considered in a free-space condition, and reflections from the ground are not considered. This approximation is used since the sound source (SRM) is located close to the ground and the measurements are carried out in free-field distance, while reflections will affect more the measurements at reverberant field distances (farther away). Moreover, for a rigid ground, the directivity of the sound field is most affected, but not so much the sound power [32].

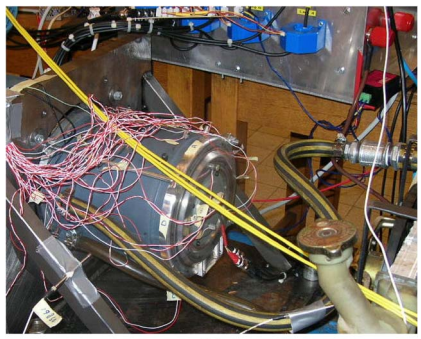

(a)

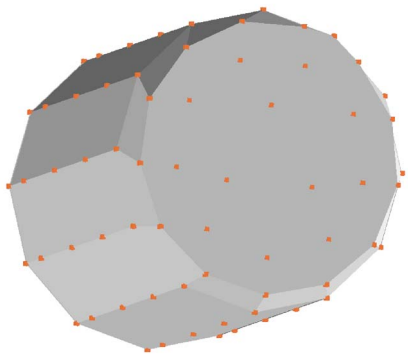

(b)

Fig. 5. Test bench with SRM and accelerometer locations. (a) Test setup: SRM and attached accelerometers on surface. (b) Accelerometer positions on 8/6 SRM surface.

TABLE I
EXPERIMENT CONDITIONS FOR SRM

Run	Speed	Load	DC bus	Ref. current
1	2044 RPM	0 N.m	300 V	15.5 A
2	3950 RPM	0 N.m	300 V	13 A
3	100 to 1000 RPM	5 to 1.5 N.m	300 V	10 A

IV. EXPERIMENTAL RESULTS AND SIMULATION

To validate the simulation models, experimental tests are performed on a test bench [see Fig. 5(a)] containing the 8/6 SRM with a dc machine as variable load. The SRM is controlled using hysteresis current control, and each of the four phases is activated using asymmetric half-bridge converters. Two different running conditions and a run-up are carried out. The main running conditions are detailed in Table I. Due to the commuting nature of hysteresis current control, there is no fixed switching frequency for the power electronics—the frequency is dependent on the rotational speed, and its effect will be present in the current harmonics.

Runs 1 and 2 were used to compare simulated and measured data, while the run-up is mainly used to obtain and confirm critical operational characteristics, such as the harmonics and

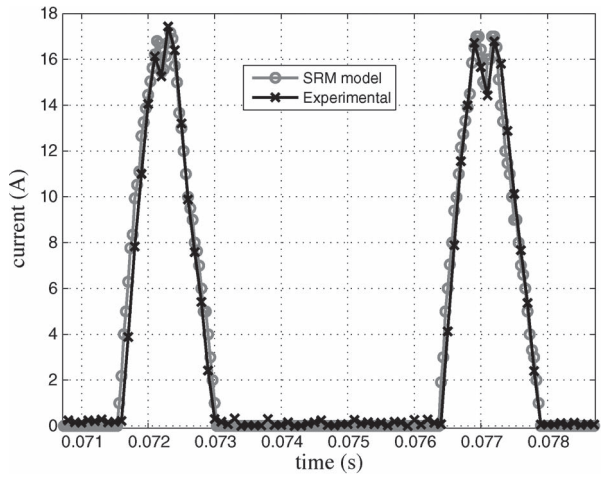

Fig. 6. SRM phase current at 2044 r/min. ○: Simulation model. ×: Experimental measurement.

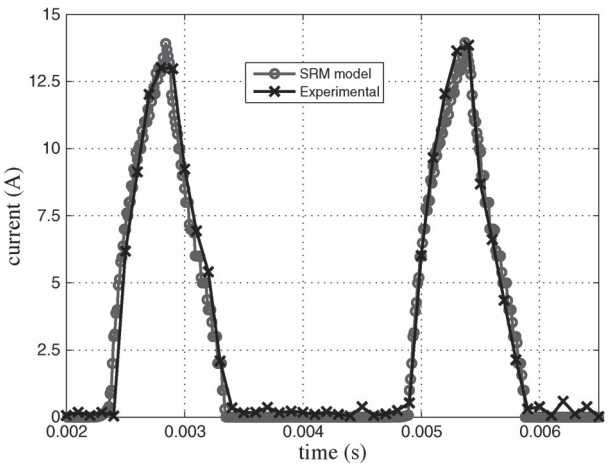

Fig. 7. SRM phase current at 3950 r/min. ○: Simulation model. ×: Experimental measurement.

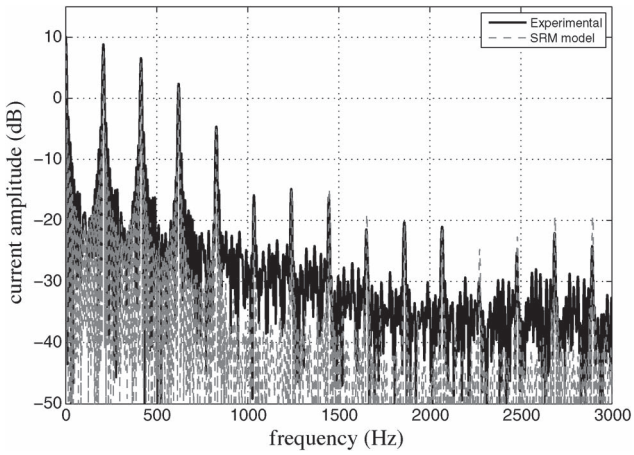

Fig. 8. Spectrum of the phase current at 2044 r/min. (− −): Simulation model. (—): Experimental measurement (run 1).

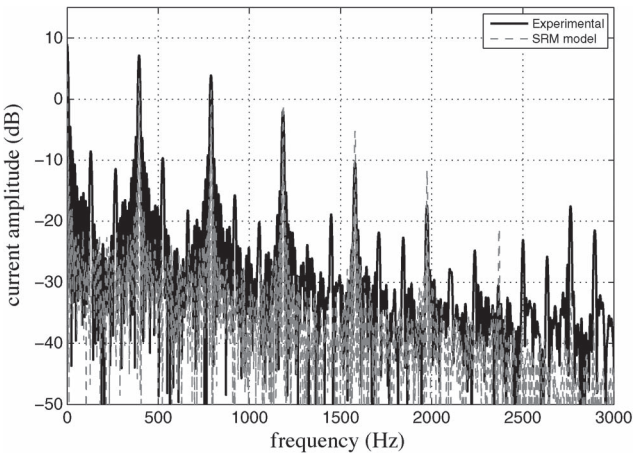

Fig. 9. Spectrum of the phase current at 3950 r/min. (− −): Simulation model. (—): Experimental measurement (run 2).

the stator resonance frequency. The run-up acceleration was controlled by reducing the load while keeping the reference current and activation angles constant.

Vibration and sound pressure data were acquired in the test setup by means of accelerometers measuring accelerations normal to the surface, covering the whole motor casing. A total of 72 measurement points were chosen for the acquisition, and the points are shown in Fig. 5(b). Five microphones placed around the test setup were used to measure acoustic pressure levels. Their locations were chosen in a way to measure possible secondary sources of noise, such as the radiator fan from the cooling circuit, power electronics, and the load motor. Additionally, phase current, torque, and angular velocity data were also acquired directly from the digital control system. To evaluate the precision of the 1-D simulation model, the same experimental conditions were applied to a simulation run, and the results were compared. Figs. 6 and 7 compare the simulation model with the experimental results, for both 2044 and 3950 r/min. Since the magnetic forces acting on the stator are directly related to the phase currents, accuracy in predicting current waveforms is essential. Furthermore, the frequency spectrum of the phase currents needs to be evaluated, as it should contain all the harmonic components present in the real system. The expected harmonic components in the phase current are related to the number of rotor poles. In an 8/6 SRM, phases are activated six times per revolution [8], leading to sixth-order harmonics and their multiples. For a given angular velocity, the harmonic frequencies can be calculated with

$$f_h = \frac{\dot{\theta}_{\mathrm{r/min}} \cdot n_{rp} \cdot n_h}{60} \tag{10}$$

where $\dot{\theta}_{\mathrm{r/min}}$ is the angular velocity in revolutions per minute (r/min), n_{rp} is the number of rotor poles, and n_h are the harmonic multiples. Figs. 8 and 9 show the frequency spectrum of the simulated and measured phase currents, where the harmonics are clearly visible.

The surface acceleration obtained experimentally can be a good indicator of the operational characteristics of the motor and can also help understand the acoustic behavior of the system. The spectra of the surface vibration from both experiment and simulation are shown in Fig. 10 for run 1 (at 2044 r/min), and in Fig. 11, the same curves are shown for the motor in run 2 (at 3950 r/min). From the graphs, some important information can already be retrieved. At lower frequencies

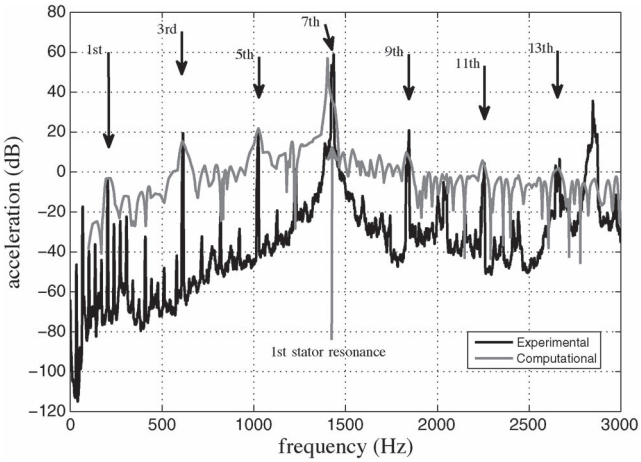

Fig. 10. Measured spectrum of the 8/6 SRM surface acceleration at 2044 r/min with the odd-numbered multiple of sixth harmonics and resonance shown. (▬): Simulation model. (▬): Experimental measurement (run 1).

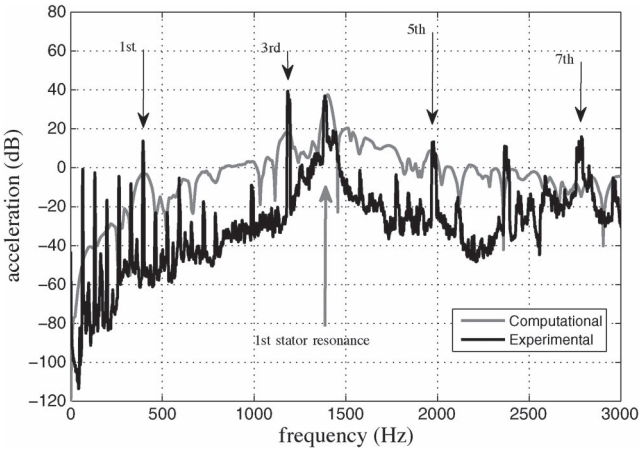

Fig. 11. Measured spectrum of the 8/6 SRM surface acceleration at 3950 r/min with the odd-numbered multiple of sixth harmonics and resonance shown. (▬): Simulation model. (▬): Experimental measurement (run 2).

(below 500 Hz), there is a substantial amount of vibration at harmonics related to the rotating speed—these are caused by the misalignment between the SRM and the load and, as such, will not be addressed in this study. The dominating vibration peaks are multiples of the sixth harmonics, due to the number of rotor poles. These peaks are notably more dominant on odd-numbered multiples of that harmonic because of the coupling factors between nonadjacent phases [8].

Additionally, the first resonance of the stator can be identified at around 1400 Hz. When this resonance is excited by one of the odd-numbered harmonics, there is great amplification in the vibration of the stator (see Figs. 10 and 11). This resonance is put more into evidence with the motor run-up. A color map of the vibration in function of the motor speed and frequency is shown in Fig. 12 where the resonance frequency is clear and the harmonic components can also be seen.

The first natural frequency of the stator, computed by FEA, matches the frequency obtained operationally. Fig. 13 shows the structural model of the SRM stator and its first mode shape at 1401 Hz.

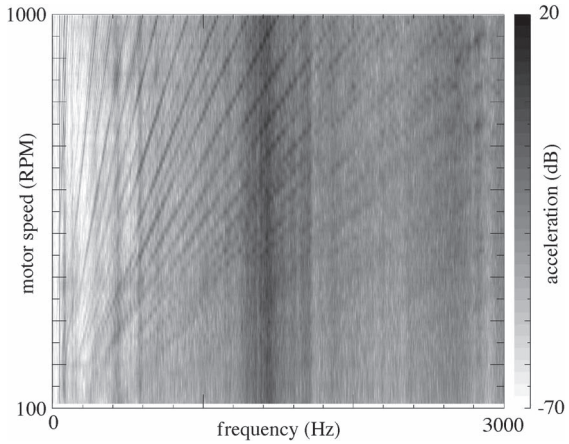

Fig. 12. SRM experimental run-up (run 3): Vibration data and first mode. The diagonal lines represent the velocity-dependent harmonics, while the vertical dark area puts in evidence a resonance at around 1400 Hz.

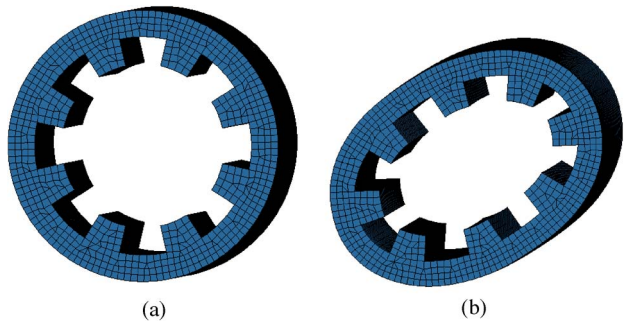

Fig. 13. SRM finite-element model. (a) Undeformed model. (b) First mode shape. (a) Stator finite-element model. (b) First vibration mode at 1401 Hz.

Having obtained the current waveforms and the structural model, the next step is to calculate the magnetic forces acting on the stator. These forces are calculated via the Maxwell stress tensor with the 2-D electromagnetic finite-element model of the SRM. A full rotation is performed, and at each step, the appropriate current is applied to the four phases, based on the current waveforms; subsequently, the surface forces acting on the stator are obtained.

The calculated force exerted on each stator pole is divided into 14 equidistant points along the stator pole surface and is converted to the frequency domain via discrete Fourier transform, taking care to keep the phase information. The frequency range of interest is up to 3 kHz since the most dominant vibration mode is located around 1.4 kHz and the harmonics have a more predominant amplitude around that range.

A modal forced response is calculated based on the simulated forces and structural stator model, and the resulting surface accelerations are used as boundary condition for the BEM simulation. Subsequently, the boundary element simulation is performed. The radiated sound power levels were calculated and can be compared with the measured sound power levels. Figs. 14 and 15 show the comparison between measurements and computational results. The peaks due to the harmonic excitations, which constitute the most relevant part of the noise, are clearly matched, particularly for the case at 2044 r/min. In both cases, there is an overestimation of the power in between

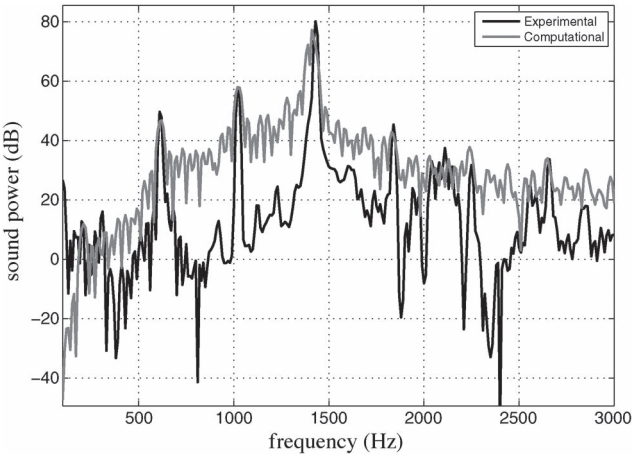

Fig. 14. Comparison of the sound power level between (—) experimental measurement and (▬) simulated results for the SRM rotating at 2044 r/min.

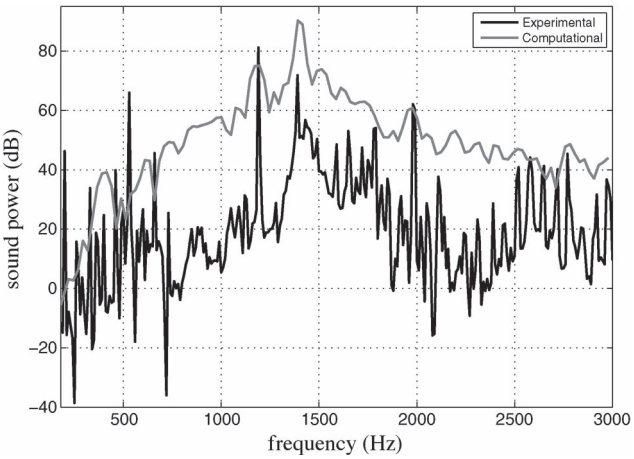

Fig. 15. Comparison of the sound power level between (—) experimental measurement and (▬) simulated results for the SRM rotating at 3950 r/min.

harmonic peaks. This difference is attributed to the fact that the casing, which includes the cooling jacket, was not modeled.

V. Summary, Conclusion, and Future Work

This paper presented a multiphysics analysis to predict the acoustic radiation properties of an SRM. The SRM model is created by means of lookup tables that contain magnetic characteristics of the motor, obtained by means of 2-D magnetic FEA. A 1-D multidomain system is used to simulate the motor under the required conditions, and phase current and rotor position can be extracted from it.

The vibroacoustic problem is solved by means of FEA and BEM, using as excitation the forces obtained through stress tensor integrals.

Simulation results were compared with experimental data gathered from the test setup of an 8/6 SRM. Phase currents from the SRM model are in agreement with those obtained experimentally, and the simulated sound power levels were compatible with those obtained experimentally, particularly regarding the harmonic components, which contain the most dominant levels of noise [20]. Discrepancies in those results are attributed mainly to the fact that the casing was not modeled as part of the structural system.

The multiphysics approach proposed in the analysis consists of a chain of simulations, coupled bidirectionally and unidirectionally. Each step in the simulation process allows for system inputs or modifications, such as geometry, material changes, or control strategies, and thus, it can be used as a powerful tool, to predict the acoustic behavior of the motor in an early design stage, being particularly useful in applications where noise emission is relevant, such as the automotive industry.

Currently, the described procedure is still computationally costly, taking a reasonable amount of time, especially when computing the force density on the stator poles. Future works aim at making this process faster and more automatized, by using lookup tables that contain magnetic force data for the full range of operations. Furthermore, structural models of the casing and cooling jacket with fluid shall also be added to the vibroacoustic system.

References

[1] M. Krishnamurthy, C. Edrington, A. Emadi, P. Asadi, M. Ehsani, and B. Fahimi, "Making the case for applications of switched reluctance motor technology in automotive products," *IEEE Trans. Power Electron.*, vol. 21, no. 3, pp. 659–675, May 2006.

[2] R. Inderka, M. Menne, and R. De Doncker, "Control of switched reluctance drives for electric vehicle applications," *IEEE Trans. Ind. Electron.*, vol. 49, no. 1, pp. 48–53, Feb. 2002.

[3] I. Husain and S. Hossain, "Modeling, simulation, and control of switched reluctance motor drives," *IEEE Trans. Ind. Electron.*, vol. 52, no. 6, pp. 1625–1634, Dec. 2005.

[4] D. Panda and V. Ramanarayanan, "Reduced acoustic noise variable dc-bus-voltage-based sensorless switched reluctance motor drive for HVAC applications," *IEEE Trans. Ind. Electron.*, vol. 54, no. 4, pp. 2065–2078, Aug. 2007.

[5] L. Chen and W. Hofmann, "Speed regulation technique of one bearingless 8/6 switched reluctance motor with simpler single winding structure," *IEEE Trans. Ind. Electron.*, vol. 59, no. 6, pp. 2592–2600, Jun. 2012.

[6] J. Florentin, F. Durieux, Y. Kuriyama, T. Yamamoto, M. DeBruin, S. Jordan, J. Han, G. Barber, Q. Zou, and X. Sun, "Electric motor noise in a lightweight steel vehicle," in *Proc. SAE Noise Vibration Conf. Exhib.*, 2011, vol. 1, p. 234.

[7] K. Vijayakumar, R. Karthikeyan, S. Paramasivam, R. Arumugam, and K. Srinivas, "Switched reluctance motor modeling, design, simulation, and analysis: A comprehensive review," *IEEE Trans. Magn.*, vol. 44, no. 12, pp. 4605–4617, Dec. 2008.

[8] J. Fiedler, K. Kasper, and R. De Doncker, "Calculation of the acoustic noise spectrum of SRM using modal superposition," *IEEE Trans. Ind. Electron.*, vol. 57, no. 9, pp. 2939–2945, Sep. 2010.

[9] J. Li and Y. Cho, "Investigation into reduction of vibration and acoustic noise in switched reluctance motors in radial force excitation and frame transfer function aspects," *IEEE Trans. Magn.*, vol. 45, no. 10, pp. 4664–4667, Oct. 2009.

[10] W. Cai, P. Pillay, Z. Tang, and A. Omekanda, "Low-vibration design of switched reluctance motors for automotive applications using modal analysis," *IEEE Trans. Ind. Appl.*, vol. 39, no. 4, pp. 971–977, Jul./Aug. 2003.

[11] J. Krotsch and B. Piepenbreier, "Radial forces in external rotor permanent magnet synchronous motors with non-overlapping windings," *IEEE Trans. Ind. Electron.*, vol. 59, no. 5, pp. 2267–2276, May 2012.

[12] J. Li, X. Song, and Y. Cho, "Comparison of 12/8 and 6/4 switched reluctance motor: Noise and vibration aspects," *IEEE Trans. Magn.*, vol. 44, no. 11, pp. 4131–4134, Nov. 2008.

[13] M. van der Giet, E. Lange, D. Correa, I. Chabu, S. Nabeta, and K. Hameyer, "Acoustic simulation of a special switched reluctance drive by means of field-circuit coupling and multiphysics simulation," *IEEE Trans. Ind. Electron.*, vol. 57, no. 9, pp. 2946–2953, Sep. 2010.

[14] N. Bracikowski, M. Hecquet, P. Brochet, and S. Shirinskii, "Multi-physics modeling of a permanent magnet synchronous machine by using lumped models," *IEEE Trans. Ind. Electron.*, vol. 59, no. 6, pp. 2426–2437, Jun. 2012.

[15] J. Le Besnerais, A. Fasquelle, M. Hecquet, J. Pelle, V. Lanfranchi, S. Harmand, P. Brochet, and A. Randria, "Multiphysics modeling: Electro-vibro-acoustics and heat transfer of PWM-fed induction machines," *IEEE Trans. Ind. Electron.*, vol. 57, no. 4, pp. 1279–1287, Apr. 2010.
[16] T. Miller, "Optimal design of switched reluctance motors," *IEEE Trans. Ind. Electron.*, vol. 49, no. 1, pp. 15–27, Feb. 2002.
[17] W. Ding and D. Liang, "A fast analytical model for an integrated switched reluctance starter/generator," *IEEE Trans. Energy Convers.*, vol. 25, no. 4, pp. 948–956, Dec. 2010.
[18] X. Xue, K. Cheng, T. Ng, and N. Cheung, "Multi-objective optimization design of in-wheel switched reluctance motors in electric vehicles," *IEEE Trans. Ind. Electron.*, vol. 57, no. 9, pp. 2980–2987, Sep. 2010.
[19] S. Faid, P. Debal, and S. Bervoets, "Development of a switched reluctance motor for automotive traction applications," in *Proc. 25th World Battery, Hybrid, Fuel Cell Elect. Veh. Symp. Exhib.*, Shenzhen, China, 2010.
[20] O. Ilsen, N. Vaninbroukx, B. Van Hooreweder, P. Sas, S. Faid, J. Anthonis, and P. Aarnoutse, "Analysis of radiated noise in electric vehicles with a switched reluctance traction motor," in *Proc. 8th Int. Automot. Congr.*, 2011.
[21] P. Zhang, P. Cassani, and S. Williamson, "An accurate inductance profile measurement technique for switched reluctance machines," *IEEE Trans. Ind. Electron.*, vol. 57, no. 9, pp. 2972–2979, Sep. 2010.
[22] H. Torkaman, E. Afjei, and M. Toulabi, "New double-layer-per-phase isolated switched reluctance motor: Concept, numerical analysis, and experimental confirmation," *IEEE Trans. Ind. Electron.*, vol. 59, no. 2, pp. 830–838, Feb. 2012.
[23] B. Bilgin, U. Krishnamurthy, and A. Emadi, "Design considerations for switched reluctance machines with higher number of rotor poles," *IEEE Trans. Ind. Electron.*, vol. 59, no. 10, pp. 3745–3756, Oct. 2012.
[24] K. Geldhof, A. Van den Bossche, and J. Melkebeek, "Rotor-position estimation of switched reluctance motors based on damped voltage resonance," *IEEE Trans. Ind. Electron.*, vol. 57, no. 9, pp. 2954–2960, Sep. 2010.
[25] C. Mademlis and I. Kioskeridis, "Gain-scheduling regulator for high-performance position control of switched reluctance motor drives," *IEEE Trans. Ind. Electron.*, vol. 57, no. 9, pp. 2922–2931, Sep. 2010.
[26] H. Hannoun, M. Hilairet, and C. Marchand, "Design of an SRM speed control strategy for a wide range of operating speeds," *IEEE Trans. Ind. Electron.*, vol. 57, no. 9, pp. 2911–2921, Sep. 2010.
[27] S. Lukic and A. Emadi, "State-switching control technique for switched reluctance motor drives: Theory and implementation," *IEEE Trans. Ind. Electron.*, vol. 57, no. 9, pp. 2932–2938, Sep. 2010.
[28] W. Heylen and P. Sas, "Modal analysis theory and testing," Dept. Werktuigkunde, Katholieke Univer. Leuven, Leuven, Belgium, 2006.
[29] S. Li, "An efficient technique for multi-frequency acoustic analysis by boundary element method," *J. Sound Vib.*, vol. 283, no. 3–5, pp. 971–980, May 2005.
[30] P. Fiala, J. Huijssen, B. Pluymers, R. Hallez, and W. Desmet, "Fast multipole BEM modeling of head related transfer functions of a dummy head and torso," in *Proc. ISMA Conf.*, Leuven, Belgium, 2010, pp. 2301–2316.
[31] M. S. Lenzi, S. Lefteriu, H. Beriot, and W. Desmet, "A fast frequency sweep approach using Padé approximations for solving Helmholtz finite element models," *J. Sound Vib.*, vol. 332, no. 8, pp. 1897–1917, Apr. 2013.
[32] H. Brick, R. Piscoya, M. Ochmann, and P. Költzsch, "A hybrid LES-BEM method for the calculation of combustion noise above an infinite plane," in *Proc. Euronoise*, Tampere, Finland, 2006.

Fábio L. M. dos Santos was born in Rio Claro, Brazil, in 1985. He received the B.Sc. degree in control and automation engineering from the University of Campinas, Campinas, Brazil, and the M.Sc. degree from the Politecnico di Torino, Turin, Italy, in 2008.

He is currently a Research Engineer with LMS International, Leuven, Belgium, as a Fellow of the IMESCON Project, which is a European Commission ITN Marie Curie Programme, and he is also a Ph.D. Researcher at the Instituto Tecnológico de Aeronáutica, São José dos Campos, Brazil.

Jan Anthonis received the M.S. degree in mechanical engineering and the Ph.D. degree from the Katholieke Universiteit (KU) Leuven, Leuven, Belgium, in 1994 and 2000, respectively.

He worked for seven years as a Postdoctoral Researcher at the same university and then moved to the private company LMS International, Leuven, which has been part of Siemens since 2013. At LMS, he is responsible for the research subjects mechatronics and control, and model-based system engineering with application domains (hybrid)-electrical vehicles, vehicle dynamics, and agricultural machinery. He is also a Visiting Professor at the KU Leuven.

Francesco Naclerio was born in Belluno, Italy, in 1987. He received the B.Sc. degree in mechanical engineering and the M.Sc. degree from the Politecnico di Milano, Milan, Italy, in 2010 and 2012, respectively.

He is currently a trainee at LMS International, Leuven, Belgium, as a Fellow under the Flanders' Drive Electric Powetrain project, where he worked on transfer path analysis methods for switched reluctance motors. His main research interests are building and validating knowledge about the system requirements for electric vehicles.

Johan J. C. Gyselinck (M'05) received the M.S. degree in electrical and mechanical engineering and the Ph.D. degree in applied sciences from Ghent University, Gent, Belgium, in 1991 and 2000, respectively.

From 2000 to 2004, he was a Postdoctoral Researcher at the Applied and Computational Electromagnetics research unit of the University of Liège, Liège, Belgium. He is currently an Associate Professor with the Université Libre de Bruxelles, Brussels, Belgium, and his research mainly concerns the numerical computation of magnetic fields, the simulation and control of electrical machines and drives, and renewable energy systems.

Herman Van der Auweraer (M'77) received the M.Sc. degree in electronic engineering and the Ph.D. degree in engineering science from the Katholieke Universiteit (KU) Leuven, Leuven, Belgium, in 1980 and 1987, respectively.

He still is a part-time Professor with KU Leuven. Since 1986, he has been with LMS International, Leuven, one of the earliest KU Leuven spin-offs, developing advanced testing and simulation tools for mechatronic product design engineering. His research focus is acoustics, sound quality, and system identification. As Research Director, he is responsible for the company's technology strategy, intellectual property rights policies, university cooperation, and the definition of strategic research programs.

Luiz C. S. Góes received the B.S. degree in electrical engineering and the M.S. degree in physics from the Aeronautical Institute of Technology (ITA), São José dos Campos, Brazil, in 1975 and 1978, respectively, and the Ph.D. degree in electrical engineering from the University of Wisconsin, Madison, WI, USA, in 1986.

He has been with ITA since 1976, where he is currently a Full Professor in the Mechanical Engineering Department. His main research interests are dynamic modeling, system identification, and control of aeronautical systems.